COMMUNICATIONS

Femtosecond time-resolved photoelectron–photoion coincidence imaging studies of dissociation dynamics

J. A. Davies[a] and J. E. LeClaire
Combustion Research Facility, Sandia National Laboratories, P.O. Box 969, Livermore, California 94551-0969

R. E. Continetti
Department of Chemistry and Biochemistry, University of California, San Diego, 9500 Gilman Drive, La Jolla, California 92093-0314

C. C. Hayden[b]
Combustion Research Facility, Sandia National Laboratories, P.O. Box 969, Livermore, California 94551-0969

(Received 25 January 1999; accepted 22 April 1999)

We present the first results using a new technique that combines femtosecond pump–probe methods with energy- and angle-resolved photoelectron–photoion coincidence imaging. The dominant dissociative multiphoton ionization (DMI) pathway for NO_2 at 375.3 nm is identified as three-photon excitation to a repulsive potential surface correlating to $NO(C\ ^2\Pi)+O(^3P)$ followed by one-photon ionization to $NO^+(X\ ^1\Sigma^+)$. Dissociation along this surface is followed on a femtosecond timescale. © *1999 American Institute of Physics.* [S0021-9606(99)02525-8]

The capability for following photodissociation dynamics directly in time is an exciting development in chemical dynamics brought about by the availability of femtosecond lasers. Initially, femtosecond time-resolved laser-induced fluorescence[1] and absorption[2] techniques were applied as probes of dissociation, but subsequently time-resolved photoionization probes, using mass spectrometry and photoelectron spectroscopy, were developed and applied to a substantially wider range of molecules and more complicated molecular systems.[1,3–5] Time-resolved mass spectrometric techniques that provide one-dimensional photofragment energy and angular resolution have also been developed for studies of reactions with multiple dissociation pathways.[6] However, when using photoionization probes, it is advantageous to detect both the photoion and photoelectron in coincidence,[7] since both particles provide important information on the dissociation event. This communication presents a new femtosecond time-resolved photoionization probe technique that combines photoelectron–photoion coincidence (PEPICO)[8,9] detection with three-dimensional energy- and angle-resolved imaging.[10,11] The present studies follow the time evolution of the dissociation process that occurs during dissociative multiphoton ionization (DMI) of NO_2 induced by femtosecond laser pulses centered at 375.3 nm (3.30 eV). This technique also provides time-resolved identification of the dissociation products and ionization pathway.

There have been a tremendous number of previous studies on dissociation and ionization processes in NO_2.[12–14] Recently, there has been increased interest in the femtosecond dynamics of these processes,[15] particularly multiphoton ionization.[16,17] Other work at 375 nm (Ref. 16) found that DMI strongly dominates over simple parent ionization. This is an interesting result since parent ionization (9.59 eV) is accessible by three-photon absorption, whereas four photons are required for DMI (12.37 eV). The DMI channel was postulated to be one-photon dissociation to ground-state NO+O (3.12 eV), followed by three-photon ionization to NO^+. However, the present work demonstrates that a different DMI channel dominates.

A schematic diagram of the experimental setup is shown in Fig. 1. Laser pulses of 100 fs duration (determined from the single-shot autocorrelation width of 160 fs) are produced from a regeneratively amplified titanium sapphire laser system (Clark MXR), operating at 2.2 kHz. The pulses are frequency doubled to a peak wavelength of 375.3 nm using a BBO crystal. The cross-correlation between the fundamental and second harmonic is comparable to the autocorrelation width of the fundamental. The laser beam is split into two paths so that one pulse may be time-delayed with respect to the other. The two beams are then recombined and focused into an ultra-high vacuum chamber to an intensity of approximately $10^{12}\,W\,cm^{-2}$.

The femtosecond laser beam is crossed with a continuous molecular beam (2% NO_2 in Ar) in the horizontal plane. The laser pulses dissociate and ionize the molecules. After an ionization event, the electron is accelerated in a direction perpendicular to both the laser and molecular beams and towards a time- and position-sensitive detector,[18] while the ion

[a]Visiting Research Scientist from Department of Chemistry and Biochemistry, University of California, San Diego, 9500 Gilman Drive, La Jolla, CA 92093-0314.
[b]Author to whom correspondence should be addressed.

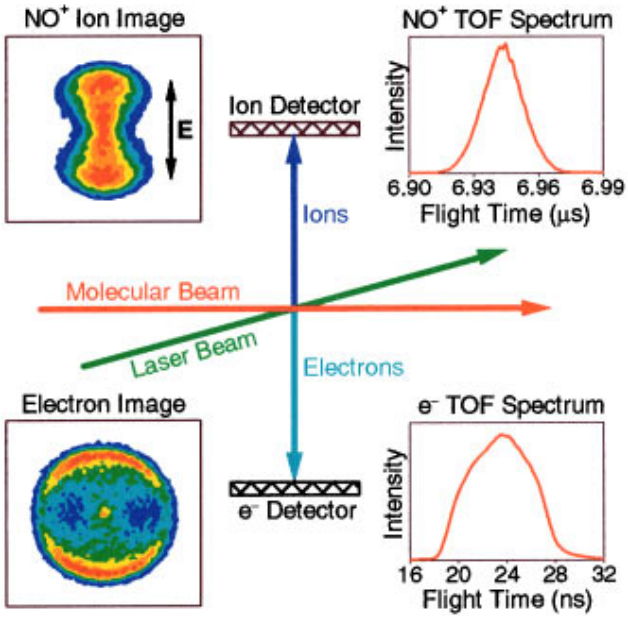

FIG. 1. Schematic diagram of the femtosecond PEPICO imaging apparatus. Detector images and time-of-flight (TOF) spectra for NO^+ ions and coincident electrons are shown for the DMI of NO_2 at 375.3 nm with zero time delay. Each TOF spectrum is measured along the direction of acceleration of the charged particles, while each image is recorded in a plane perpendicular to this direction. The arrow labeled **E** indicates the direction of the laser polarization, parallel to the detector planes. The most intense signal in the images is shown in red.

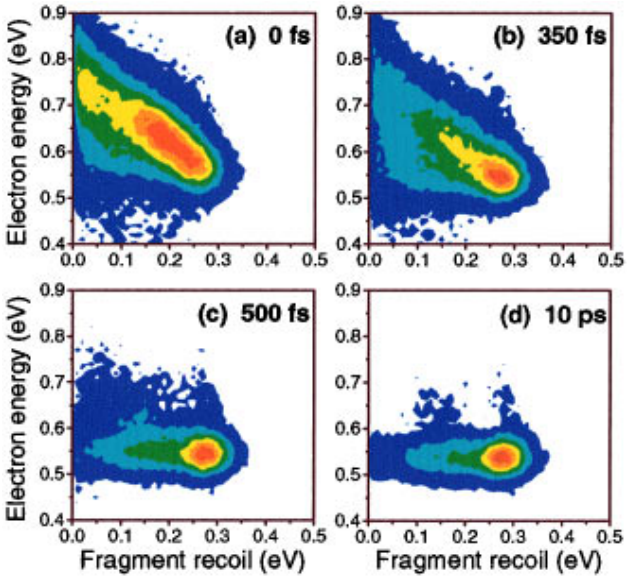

FIG. 2. Energy correlation spectra for the DMI of NO_2 at 375.3 nm, using time delays of (a) 0 fs, (b) 350 fs, (c) 500 fs, and (d) 10 ps. The intensity distribution is plotted on a linear scale with red representing the most intense features and dark blue representing the least intense. The lowest 5% of the signal is plotted in white.

is accelerated in the opposite direction towards a similar detector. The detector records the arrival time, and hence velocity, of the particle in one dimension, while the position supplies the other two dimensions of the particle velocity. In the case of the ion, the arrival time also provides mass selection. The particles are detected in coincidence, such that the ion–electron pair originates from the same ionization event. This requires that less than one ionization event occurs per laser shot (~0.01 events per pulse) to ensure against false coincidence events. After the detection of many true coincident events, complete 3D ion and electron velocity distributions are obtained due to the 4π acceptance solid angles of both detectors. This is the first apparatus that measures the full 3D energy and angular distributions for coincident photofragment ions and photoelectrons.

The initial observation from these experiments is that over 90% of the ions produced are NO^+. Hence, DMI is the major ionization pathway, in agreement with previous work.[16] Data from the DMI of NO_2 at 375.3 nm are shown in Fig. 1, with the position and arrival-time distributions plotted separately for the coincident NO^+ ions and electrons. The data were taken with the laser polarization perpendicular to the axis of the ion and electron flight paths. Using the position and arrival time together, the recoil velocity vectors for the photofragment and photoelectron are calculated for each detected event. These data can subsequently be sorted in many different ways to display particular features of the dissociation dynamics, such as energy or angular distributions.

A particularly informative way to display the ion and electron data is as an energy correlation spectrum.[19] This plots the joint probability distribution of the total fragment recoil energy and the coincident electron kinetic energy for all ionization events (Fig. 2). The total fragment recoil is the sum of the measured NO^+ ion recoil and the corresponding neutral O-atom fragment recoil, determined from momentum conservation. A vertical slice through one of these diagrams is a photoelectron spectrum for photofragments with a particular recoil energy. A diagonal line represents constant total (fragment recoil + electron) kinetic energy. Figure 2 shows a sequence of energy correlation spectra for the DMI of NO_2 at 375.3 nm with various time delays between the pump and probe laser pulses. The spectrum for 0 fs is equivalent to one obtained with a single laser pulse. The plots with nonzero time delays have had the signals due to each individual laser pulse subtracted from them, so the signal plotted is only that resulting from excitation by the first pulse followed by ionization with the second pulse.

Figures 2(a) and 2(b) show energy correlation spectra for time delays of 0 and 350 fs. At these short time delays, ionization occurs during dissociation producing a broad photoelectron energy distribution. The electron kinetic energy and fragment recoil energy are inversely related, with high electron energies corresponding to low fragment energies and vice versa, such that the total kinetic energy is conserved. This results in the diagonal intensity band seen in Figs. 2(a) and 2(b). Figures 2(c) and 2(d) show energy correlation spectra for time delays of 500 fs and 10 ps. By 500 fs the dissociation of excited NO_2 appears to be complete because the electron energy distribution is narrow and does not vary with the fragment recoil energy. These results are characteristic of ionization of a freely recoiling fragment. Horizontal stripes are observed in the energy correlation spectra because NO fragments are produced with a broad rotational energy distribution that is conserved in the subsequent ionization.

Figure 3 presents measurements of the strongly asym-

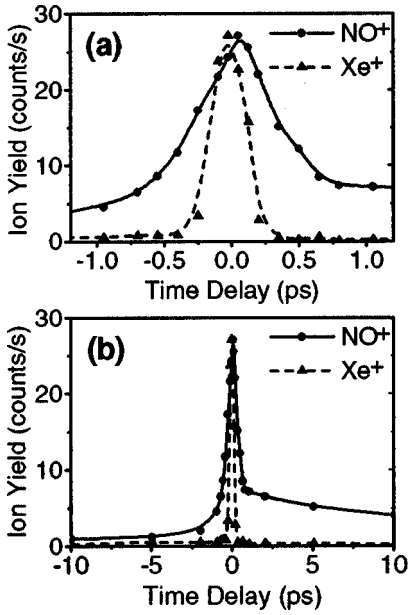

FIG. 3. Plot of ion yield against pump–probe time delay over ranges from (a) -1.2 to $+1.2$ ps and (b) -10 to $+10$ ps. For negative time delays, the pump pulse is weaker than the probe pulse. The solid curve shows the yield of NO^+ ions from DMI of NO_2 at 375.3 nm. The dashed curve represents the yield of Xe^+ ions from four-photon ionization of Xe. This illustrates that the nonresonant, four-photon ionization signal falls to zero before 350 fs. The xenon ionization profile is wider than the measured laser cross-correlation ($\sim$160 fs) because optical interference between the two identical laser pulses reduces the signal intensity near zero time delay.

metric yield of NO^+ ions as a function of the time delay between the excitation and ionization pulses. In comparison, the normalized signal from four-photon ionization of xenon is a narrow, symmetric peak appearing at time delays shorter than 350 fs. Prior to plotting the data, the ion signals produced by each individual pulse were subtracted. The NO^+ ion yield scan is asymmetric because the two 375.3 nm laser pulses do not have the same pulse energy. The larger NO^+ ion signal at long positive delay times occurs when the more intense pulse precedes the less intense pulse [Fig. 3(b)]. This observation suggests that the dissociative process involves a larger number of photons than the ionization. The slowly decaying signal at long time delays in the ion yield plot corresponds to ionization of free NO fragments. The rapidly decaying signal at short time delays corresponds to ionization of the dissociating NO_2. The ion yield data in Fig. 3 suggest that the dissociation process is essentially complete by 500 fs in agreement with the energy correlation spectra presented in Fig. 2.

The DMI mechanism for NO^+ production can be ascertained by first considering the energy correlation spectra at long time delays [Figs. 2(c) and 2(d)]. Since the molecule has fully dissociated before being ionized, the fragment and electron recoil energies determine the final dissociation and ionization products. The prominent peak in the photofragment recoil energy at 0.28 eV with a photoelectron energy of 0.54 eV corresponds to a total product kinetic energy of 0.82 eV. The difference between the energy of four 375.3 nm photons (13.22 eV) and the total kinetic energy (0.82 eV) is 12.40 eV, in close agreement with the lowest dissociative ionization energy of NO_2 (12.37 eV). This identifies the overall process as four-photon DMI to yield $NO^+(X\ ^1\Sigma^+) + O(^3P)$. The photofragment recoil and photoelectron energies then identify the dissociation fragments to be $NO(C\ ^2\Pi) + O(^3P)$ at an energy of 9.61 eV above the NO_2 ground-state. These photofragments are produced by three-photon dissociation. Subsequently, one-photon ionization of $NO(C\ ^2\Pi)$ yields $NO^+(X\ ^1\Sigma^+)$. This mechanism is also consistent with the time delay scan of NO^+ yield [Fig. 3(b)]. When the strong laser pulse precedes the weak pulse, a larger NO^+ signal is observed because production of $NO(C\ ^2\Pi)$ is highly favored for the strong pulse due to the high-order intensity dependence of the three-photon dissociation.

At shorter time delays, the intensity in the energy correlation spectra [Figs. 2(a) and 2(b)] is spread along a diagonal line. This diagonal feature has its maximum photofragment kinetic energy limited by the calculated recoil energy (0.30 eV) for three-photon dissociation to $NO(C\ ^2\Pi) + O(^3P)$ and the minimum electron energy similarly limited by the calculated photoelectron energy (0.54 eV) for one-photon ionization from $NO(C\ ^2\Pi)$ to $NO^+(X\ ^1\Sigma^+)$. These limits imply that the mechanism for dissociative ionization at short time delays is analogous to that at longer delays. The initial step is three-photon excitation of the NO_2 molecule to a repulsive potential surface that leads asymptotically to $NO(C\ ^2\Pi) + O(^3P)$. As the neutral molecule dissociates and the O–NO bond length increases, the fragments gain kinetic energy while losing electronic potential energy. One-photon ionization occurs while the molecule is still dissociating and the kinetic energy acquired by the NO prior to ionization appears in the NO^+ fragment. The 100 fs ionization laser pulse accesses a range of O–NO bond lengths resulting in a broad distribution in the kinetic energy of the NO^+ ions. Conservation of energy demands that low kinetic-energy NO^+ fragments (from ionization at short internuclear separations) correspond to high-energy electrons and vice versa. This leads to the diagonal features observed in the energy correlation spectra.

Other possible DMI mechanisms, such as four-photon ionization to a dissociative state of NO_2^+ or three-photon ionization to ground-state NO_2^+ followed by one-photon dissociation, are inconsistent with our results. A previous femtosecond study in this wavelength region[16] postulated that the DMI mechanism was one-photon dissociation of NO_2 followed by three-photon ionization of the ground-state NO fragment. We selected a wavelength (375.3 nm) that is two-photon resonant with $NO(D\ ^2\Sigma^+)$ from $NO(X\ ^2\Pi)$ to accentuate the contribution of this DMI channel by resonantly enhancing the ionization of ground-state NO. However, the present results demonstrate that this mechanism does not contribute significantly to the DMI. Dissociation of NO_2 at the one-photon level would produce a maximum fragment recoil of 0.18 eV and three-photon ionization of $NO(X\ ^2\Pi)$ would produce electrons with 0.65 eV kinetic energy. These energies are inconsistent with the features seen in the energy correlation spectra (Fig. 2).

In summary, this communication presents the first results using a new femtosecond time-resolved, 3D PEPICO technique. The DMI of NO_2 is investigated using two time-delayed pulses at 375.3 nm. The dominant channel is identi-

fied as three-photon excitation to a repulsive state of NO_2 that correlates to $NO(C\ ^2\Pi)+O(^3P)$, followed by one-photon ionization to $NO^+(X\ ^1\Sigma^+)$. For a time scale shorter than 500 fs, the final ionization step occurs during the dissociation of NO_2, while on a longer time scale the dissociation is complete and the ionization occurs from free $NO(C\ ^2\Pi)$. Further studies will address the wavelength dependence of the DMI process and examine the correlated photofragment and photoelectron angular distributions.

ACKNOWLEDGMENTS

The authors are grateful to David W. Chandler for many valuable discussions throughout the course of this work. We also wish to thank Mike Gutzler for his expert technical assistance. This work is supported by the U.S. Department of Energy, Office of Basic Energy Sciences, Division of Chemical Sciences.

[1] A. H. Zewail, *Femtochemistry* (World Scientific, Singapore, 1994), Vols. I and II.
[2] J. H. Glownia, J. A. Misewich, and P. P. Sorokin, J. Chem. Phys. **92**, 3335 (1990).
[3] D. R. Cyr and C. C. Hayden, J. Chem. Phys. **104**, 771 (1996).
[4] B. J. Greenblatt, M. T. Zanni, and D. M. Neumark, Science **276**, 1675 (1997).
[5] V. Blanchet and A. Stolow, J. Chem. Phys. **108**, 4371 (1998).
[6] T. Baumert, S. Pedersen, and A. H. Zewail, J. Phys. Chem. **97**, 12447 (1993); P. Y. Cheng, D. Zhong, and A. H. Zewail, J. Chem. Phys. **105**, 6216 (1996); D. Zhong and A. H. Zewail, J. Phys. Chem. **102**, 4031 (1998).
[7] V. Stert, W. Radloff, Th. Freudenberg, F. Noack, I. V. Hertel, C. Jouvet, C. Dedonder-Lardeux, and D. Solgadi, Europhys. Lett. **40**, 515 (1997).
[8] C. J. Danby and J. H. D. Eland, Int. J. Mass Spectrom. Ion Phys. **8**, 153 (1972).
[9] I. Powis, J. Chem. Phys. **99**, 3436 (1993).
[10] J. Ullrich, R. Moshammer, R. Dörner, O. Jagutzki, V. Mergel, H. Schmidt-Böcking, and L. Spielberger, J. Phys. B **30**, 2917 (1997), and references therein.
[11] K. A. Hanold, M. C. Garner, and R. E. Continetti, Phys. Rev. Lett. **77**, 3335 (1996).
[12] K. S. Haber, J. W. Zwanziger, F. X. Campos, R. T. Wiedmann, and E. R. Grant, Chem. Phys. Lett. **144**, 58 (1988), and references therein.
[13] D. C. Robie, M. Hunter, J. L. Bates, and H. Reisler, Chem. Phys. Lett. **193**, 413 (1992), and references therein.
[14] K. Shibuya, S. Suzuki, T. Imamura, and I. Koyano, J. Phys. Chem. A **101**, 685 (1997), and references therein.
[15] G. A. Brucker, S. I. Ionov, Y. Chen, and C. Wittig, Chem. Phys. Lett. **194**, 301 (1992).
[16] R. P. Singhal, H. S. Kilic, K. W. D. Ledingham, C. Kosmidis, T. McCanny, A. J. Langley, and W. Shaikh, Chem. Phys. Lett. **253**, 81 (1996).
[17] K. Vijayalakshmi, C. P. Safvan, G. Ravinda Kumar, and D. Mathur, Chem. Phys. Lett. **270**, 37 (1997).
[18] J. V. Vallerga, G. C. Kaplan, O. H. W. Siegmund, M. Lampton, and R. F. Malina, IEEE Trans. Nucl. Sci. **NS-36**, 881 (1989).
[19] R. E. Continetti, Int. Rev. Phys. Chem. **17**, 227 (1998).